



This is a repository copy of *Taguchi-based robust design for minimising torque ripple in 6-slot/2-pole modular high-speed permanent magnet motor with manufacturing tolerances*.

White Rose Research Online URL for this paper:

<https://eprints.whiterose.ac.uk/216669/>

Version: Published Version

Article:

Xiang, D. orcid.org/0000-0002-0465-3688, Zhu, Z.Q. orcid.org/0000-0001-7175-3307, Liang, D. orcid.org/0000-0002-1574-9810 et al. (2 more authors) (2024) Taguchi-based robust design for minimising torque ripple in 6-slot/2-pole modular high-speed permanent magnet motor with manufacturing tolerances. IET Electric Power Applications. ISSN 1751-8660

<https://doi.org/10.1049/elp2.12490>

Reuse

This article is distributed under the terms of the Creative Commons Attribution-NonCommercial-NoDerivs (CC BY-NC-ND) licence. This licence only allows you to download this work and share it with others as long as you credit the authors, but you can't change the article in any way or use it commercially. More information and the full terms of the licence here: <https://creativecommons.org/licenses/>

Takedown






If you consider content in White Rose Research Online to be in breach of UK law, please notify us by emailing eprints@whiterose.ac.uk including the URL of the record and the reason for the withdrawal request.



eprints@whiterose.ac.uk
<https://eprints.whiterose.ac.uk/>

ORIGINAL RESEARCH

Taguchi-based robust design for minimising torque ripple in 6-slot/2-pole modular high-speed permanent magnet motor with manufacturing tolerances

Dong Xiang  | Zi Qiang Zhu  | Dawei Liang  | Fan Xu  | Tianran He 

Department of Electronic and Electrical Engineering,
University of Sheffield, Sheffield, UK

Correspondence

Zi Qiang Zhu.
Email: z.q.zhu@sheffield.ac.uk

Abstract

A Taguchi-based robust design strategy is proposed to minimise the torque ripple of a 6-slot/2-pole modular high-speed permanent magnet motor in mass production, accounting for manufacturing tolerances of split gap (Δg), misalignment (Δm), and offset angle ($\Delta \alpha$). Firstly, the effects and interactions of manufacturing tolerances are calculated, indicating that Δg has the highest effect followed by Δm , positive Δg and negative Δm have a strengthening effect, and $\Delta \alpha$ has no effect, and subsequently, the worst-case scenario of manufacturing tolerances with the highest torque ripple is obtained. Afterwards, tooth circumferential positions are optimised for minimising torque ripple without jeopardising average torque, considering the tradeoff between the cases without manufacturing tolerance and with the worst-case scenario of manufacturing tolerances. As will be demonstrated, torque ripples are reduced significantly, that is, they are particularly reduced by 40% in the worst-case scenario. Under hypothetical 100 sets manufacturing tolerances as Gauss distributions, the optimised machines have significantly reduced torque ripples (maximum and average reductions are 33% and 16%, respectively) with more concentrated distribution. The correctness of the methods is verified by experimental validation.

KEYWORDS

manufacturing processes, permanent magnet motors, Taguchi methods, torque

1 | INTRODUCTION

To achieve high torque density and high efficiency, permanent magnet (PM) machines have been widely adopted [1]. However, some drawbacks affect system performance and limit the application of PM machines [1–3], particularly torque ripple, which is caused by the interactions of rotor magnetic flux and angular variation in stator magnetic reluctance (i.e. cogging torque), stator current magnetomotive forces with rotor magnet flux distribution, and stator current magnetomotive forces with angular variation in rotor magnetic reluctance [4–9].

Various methods are proposed for minimising torque ripple in the PM machine without manufacturing tolerances, such as skewing [9–14], auxiliary slots [9–11], slot opening [11–13], rotor shaping [15–17], rotor pole-arc [10–13], and rotor asymmetric flux barriers [18–20]. By way of example, skewing

is an effective method to reduce torque ripple, including the skewing for stator lamination stack, rotor PMs, and rotor magnetisation [10–13], but it usually fails due to magnetic saturation. Therefore, an improved skewing method is proposed in Ref. [14] by optimising both the current phase advanced angle and skewing angle. Another popular method to minimise torque ripple is rotor shaping, including shaping for rotor PMs [15], rotor contours [16], and both rotor PMs and contours [17]. Additionally, three configurations of asymmetric flux barriers in V-shaped-type PM machines are proposed in Ref. [18], whilst two configurations of asymmetric flux barriers in spoke-type PM machines are investigated in Ref. [19], both exhibiting excellent reduction of torque ripple.

Nevertheless, only a few methods have been examined for reducing torque ripple in PM machines with manufacturing tolerances. As explained in Refs. [21–24], the reason is that

This is an open access article under the terms of the [Creative Commons Attribution-NonCommercial-NoDerivs](https://creativecommons.org/licenses/by-nc-nd/4.0/) License, which permits use and distribution in any medium, provided the original work is properly cited, the use is non-commercial and no modifications or adaptations are made.

© 2024 The Author(s). *IET Electric Power Applications* published by John Wiley & Sons Ltd on behalf of The Institution of Engineering and Technology.

manufacturing tolerances might introduce additional harmonics into the torque ripple, which easily becomes more complicated due to local saturation and is hard to eliminate by the aforementioned methods. In Ref. [24], the torque ripple can be reduced if the split gap is chosen properly in the 12-slot/10-pole and 12-slot/14-pole PM machines with a C-core modular stator. However, this method is limited by the combination of slot and pole numbers, as well as the modular structure, for example, it has a very limited effect on the reduction of torque ripple for the E-core modular PM machines. To more generally reduce the effect of manufacturing tolerances on torque ripple, the Taguchi method is adopted in Refs. [25, 26] for minimising torque ripple. In Ref. [25], the impacts of eight combinations of manufacturing tolerances, that is, variations of airgap length, tooth width, tooth tip depth, and slot opening, on torque ripple are optimised by redesigning the armature radius, airgap length, and dimensions of the stator lamination stack and PMs in the 40-slot/44-pole PM machine. Moreover, in Ref. [26], tooth width, slot opening, and PM dimensions are optimised to reduce the torque ripple due to PM tolerances and rotor eccentricities in the 12-slot/8-pole PM machine. As demonstrated in Refs. [25, 26], the torque ripples are significantly reduced after Taguchi-based optimisation. However, since the Taguchi method is a statistical tool, it relies on the designer's experience to identify suitable design variables and conditions to achieve the desired results [25–36]. Consequently, it necessitates different strategies based on the Taguchi method for various machine topologies and manufacturing tolerances.

Therefore, a Taguchi-based robust design strategy is proposed to minimise the torque ripple in the 6-slot/2-pole modular high-speed PM (HSPM) motor, which is a popular topology for high-speed appliances [37–43] and whose torque ripple is influenced significantly by the manufacturing tolerances [40].

In this paper, the topology of the investigated 6-slot/2-pole modular HSPM motor and its manufacturing tolerances, that is, the split gap (Δg), misalignment (Δm), and offset angle ($\Delta \alpha$), are introduced. Particularly, Gauss and half-Gauss distributions of manufacturing tolerances are explained with their ranges in mass production. Next, the Taguchi-based robust design strategy is proposed, which is employed to evaluate the effects and interactions of manufacturing tolerances and identify the worst-case scenario with the highest torque ripple. Subsequently, the tooth circumferential positions are optimised for minimising torque ripple in the machines considering the tradeoff between the cases without manufacturing tolerance and with the worst-case scenario of manufacturing tolerances. Besides, adopting hypothetical 100 sets of manufacturing tolerances, the torque ripple possibilities of the optimised machines are lower and more concentrated compared to those of the original machines.

The contributions of this paper are as follows.

1. This paper reveals the relationship between manufacturing tolerances and the torque ripple, indicating that the split gap has the highest effect followed by misalignment, positive

split gap and negative misalignment have the strengthening effect, and offset angle has no effect. Subsequently, the worst-case scenario of manufacturing tolerances with the highest torque ripple can be obtained.

2. This paper also finds that the appropriate tooth circumferential positions can significantly reduce the torque ripple without jeopardising the average torque in the machine with manufacturing tolerances as Gauss distributions.

This paper is organised as follows. In Section 2, the topology of the investigated 6-slot/2-pole modular HSPM motor and its manufacturing tolerances are introduced. In Section 3, a Taguchi-based robust design is developed to minimise torque ripple by optimising tooth circumferential positions. In Section 4, torque ripple possibilities of the machines with hypothetical 100 sets of manufacturing tolerances before and after optimisation are compared. Section 5 is experimental validation and Section 6 is the conclusion.

2 | MACHINE TOPOLOGY AND MANUFACTURING TOLERANCES

2.1 | Machine topology

Figure 1 and Table 1 show the topology and main parameters of the investigated 6-slot/2-pole modular HSPM motor [27], respectively. The machine is originally designed without considering the manufacturing tolerances, where the stator is split into two segments so that the toroidal coils can be easily wound by automation. The windings have three phases (A/B/C), and each phase has two toroidal coils in parallel. The machine is designed under the brushless direct current operation.

2.2 | Manufacturing tolerances

During the assembling of the investigated 6-slot/2-pole modular HSPM motor, three manufacturing tolerances may occur, that is, the split gap (Δg) [40], misalignment (Δm) [40], and offset angle ($\Delta \alpha$).

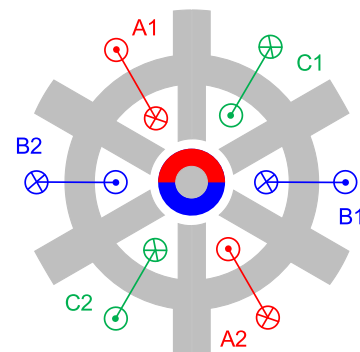


FIGURE 1 Topology of 6-slot/2-pole modular high-speed permanent magnet motor.

TABLE 1 Main parameters.

Parameter	Value	Parameter	Value
Stator outer radius, mm	27	Rotor outer radius, mm	5.25
Stator yoke width, mm	4.6	Rotor inner radius, mm	2.5
Stator tooth width, mm	4.5	PM thickness, mm	2.75
Stator tooth height, mm	8.8	PM remanence, T	1.3
Stator inner radius, mm	6.8	Magnetisation	Parallel
Number of parallel branches/phase	2	Axial length, mm	13.6
Number of turns/phase	32	Airgap length, mm	1.55
Phase current (RMS), A	12.7	Rated speed, k r/min	180

Abbreviation: PM, permanent magnet.

In Figure 2, Δg designates the split gap between the centres of two stator segments (see Figure 2a), Δm designates the magnitude of misalignment between two stator segments (see Figure 2b), and $\Delta\alpha$ represents the angle between the contacting edges of two stator segments (see Figure 2c). It is noted that Δg and Δm can exist independently, but $\Delta\alpha$ can only occur in the presence of Δg and its maximum range is limited by Δg since two stator segments may come into contact when $\Delta\alpha$ increases with a constant Δg . Their ideal values are zero. However, they may have variation ranges and possibilities during the assembly.

The possibilities of those three investigated manufacturing tolerances, which are usually subject to two distribution types, Gauss or half-Gauss distributions, as shown in Figure 3.

Firstly, Gauss distribution, Figure 3a is a type of possibility for real-valued random variables. It is used to describe the actual values that are randomly distributed on both sides of the ideal value. The possibility density function of the Gauss distribution is described by Ref. [35].

$$\varphi(x, \mu, \sigma) = \frac{1}{\sigma\sqrt{2\pi}} e^{-\frac{1}{2}\left(\frac{x-\mu}{\sigma}\right)^2} \quad (1)$$

where $\varphi(x, \mu, \sigma)$ is the possibility density of x . μ and σ are the mean and standard deviations of Gauss distribution, respectively.

Furthermore, the possibility of the range $\mu - 2\sigma \leq x \leq \mu + 2\sigma$ is used to evaluate manufacturing tolerance [23] since most mass productions (approximately 95.4%) are in this scope. Thus, twice of standard deviation (2σ) is adopted to evaluate the real effect of manufacturing tolerances in this research, with the possibility of this range being given by the following equation:

$$\Phi(\mu - 2\sigma \leq x \leq \mu + 2\sigma) = \int_{\mu-2\sigma}^{\mu+2\sigma} \varphi(x, \mu, \sigma) dx \approx 95.4\% \quad (2)$$

Secondly, the half-Gauss distribution, Figure 3b, is another common distribution, which is used to describe the actual value that is randomly distributed on one side of the ideal value. The possibility density function of the half-Gauss distribution is described in Ref. [35].

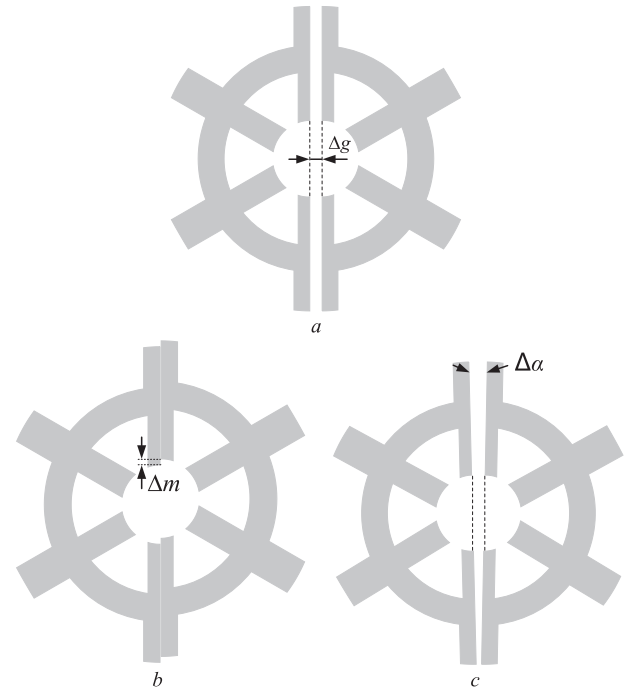


FIGURE 2 Manufacturing tolerances in 6-slot/2-pole modular high-speed permanent magnet motor. (a) Split gap (Δg), (b) misalignment (Δm), and (c) offset angle ($\Delta\alpha$).

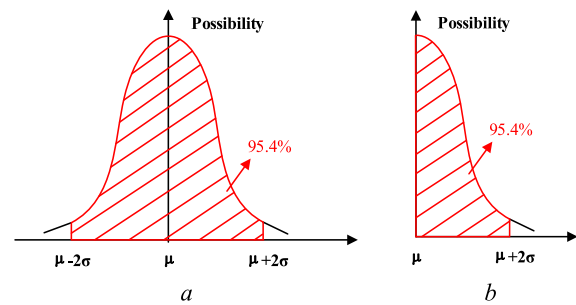


FIGURE 3 Possibilities. (a) Gauss and (b) half-Gauss.

$$\varphi_{\text{half}}(x, \mu, \sigma) = \frac{\sqrt{2}}{\sigma\pi} e^{-\frac{1}{2}\left(\frac{x-\mu}{\sigma}\right)^2} \quad \text{for } x \geq \mu \quad (3)$$

TABLE 2 Manufacturing tolerances.

Tolerance	Range (within 2σ)
Split gap (Δg), mm	Half-Gauss (0, 0.1)
Misalignment (Δm), mm	Gauss (-0.1, 0.1)
Offset angle ($\Delta \alpha$), deg.	Gauss (-0.05, 0.05)

Likewise, the possibility of two times of standard deviation (2σ) of half-Gauss distribution is given by the following equation:

$$\phi_{\text{half}}(x \leq \mu + 2\sigma) = \int_{\mu}^{x-2\sigma} \varphi_{\text{half}}(x, \mu, \sigma) \approx 95.4\% \quad (4)$$

Therefore, Δg follows the half-Gauss distribution since it only fluctuates positive side of the ideal value (zero), whilst Δm and $\Delta \alpha$ follow Gauss distributions since they fluctuate on both sides of the ideal value (zero). Even though the ranges of manufacturing tolerances are influenced by manufacture facilities and procedures, the ranges of these three tolerances, that is, $\pm 2\sigma$ of the distribution [23], adopt the conventional values in modular PM machines. The range of split gap (Δg) is 0–0.1 mm [44], the range of misalignment (Δm) is ± 0.1 mm referring to the radial movement of the modular stator in Ref. [44], and the offset angle ($\Delta \alpha$) is ± 0.05 deg. referring to variation of the angular position of assemble [23], as listed in Table 2.

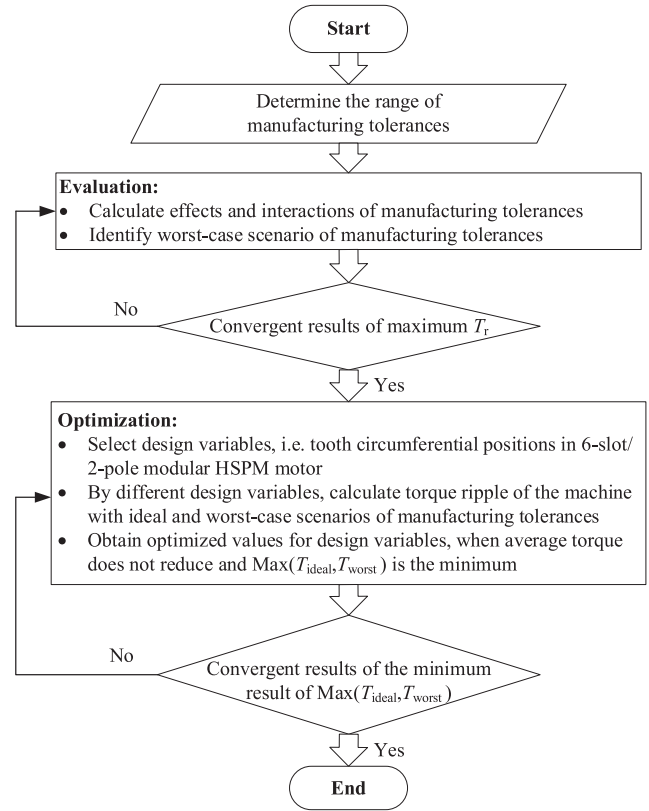
Notably, these ranges of manufacturing tolerances do not affect the feasibility of the proposed Taguchi-based robust design since the procedure is the same at any range.

3 | TAGUCHI-BASED ROBUST DESIGN FOR MINIMISING TORQUE RIPPLE

This section proposes the Taguchi-based robust design to minimise the torque ripple in the 6-slot/2-pole modular HSPM motor considering manufacturing tolerances but without jeopardising average torque. To calculate the torque ripple and average torque, the electromagnetic torques are obtained under brushless direct current operation with the ideal square current waveforms [40] using the finite element analysis (FEA).

Figure 4 outlines the complete proposed strategy processes and is described as follows.

1. The ranges of the manufacturing tolerances are determined. In most cases, two standard deviations (2σ) can be used since it includes 95.4% possibilities.
2. The worst-case scenarios of manufacturing tolerances with the highest torque ripple are evaluated. Importantly, it needs to ensure that the worst-case scenario is obtained when the highest torque ripple is convergent with increased cases due to the increased levels of manufacturing tolerances.
3. The optimisation design variables, that is, tooth circumferential positions, are selected to reduce the torque ripple, which can be chosen based on either experience or references. The objective is designed to minimise the $\max(T_{\text{ideal}}, T_{\text{worst}})$,

**FIGURE 4** Process of the Taguchi-based robust design strategy for minimising torque ripple.

T_{worst}), that is, the maximum torque ripple of the machine without tolerance and with the worst-case scenario of manufacturing tolerances. Also, the objective is obtained when the result is convergent with increased cases due to the increased levels of design variables.

3.1 | Evaluation of worst-case scenario of manufacturing tolerances

The 6-slot/2-pole modular HSPM motor has the lowest torque ripple in the ideal-case scenario (without manufacturing tolerance). However, when the manufacturing tolerances are introduced, torque ripple will be increased [40].

Table 3 shows the three levels of the manufacturing tolerances in the 6-slot/2-pole modular HSPM motor. Referring to [36], as shown in Table 4, the L27 orthogonal array in the Taguchi method can be adapted to analyse all potential effects and interactions of these three manufacturing tolerances with three levels and identify the worst-case scenario. Notably, since $\Delta \alpha$ can only occur in the presence of Δg as explained in Section 2, six cases could not have the torque ripple in Figure 5. For example, the torque ripple of the No. 1 case (Δg , Δm , and $\Delta \alpha$ are Level-1s in Table 4) does not exist in Figure 5.

Figure 5 shows the effects and the interactions of manufacturing tolerances in the 6-slot/2-pole modular HSPM

TABLE 3 Three levels of manufacturing tolerances.

	Δg , mm	Δm , mm	$\Delta\alpha$, deg.
Level-1	0	-0.1	-0.05
Level-2	0.05	0	0
Level-3	0.1	0.1	0.05

TABLE 4 Layout of the L27 orthogonal array.

	Δg	Δm	$\Delta\alpha$
1	1	1	1
2	1	1	2
...
27	3	3	3

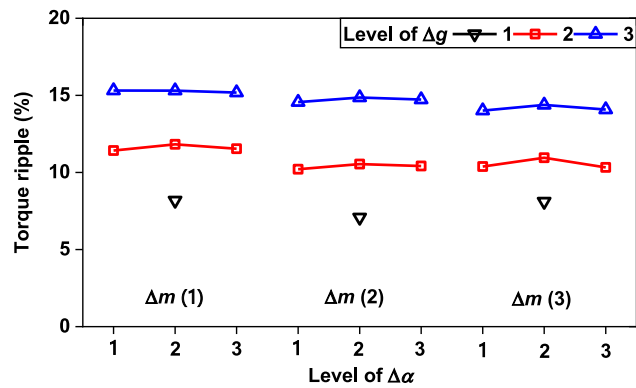


FIGURE 5 Effects and interactions of manufacturing tolerances with three levels.

motor. As can be seen, the split gap (Δg) has the greatest self and mutual effects, that is, the split gap in Level-3 (0.1 mm) will cause the highest torque ripple. Followed by the misalignment (Δm), the Level-1 (-0.1 mm) of misalignment results in the higher torque ripple when Δg is present. The reason is that Δg and $-\Delta m$ have a strengthening effect, but Δg and Δm have a weakening effect. In comparison, the offset angle ($\Delta\alpha$) almost does not have an obvious influence on torque ripple. The reason is that one side of the split gap close to the airgap is reduced and another side is increased, whilst their combined effects on torque ripple cancel each other and are equal to their mean. Therefore, positive Δg and negative Δm have a strengthening effect and $\Delta\alpha$ has no effect, and subsequently, the worst-case scenario of manufacturing tolerances is that Level-3 (0.1 mm) of Δg , Level-1 (-0.1 mm) of Δm , and any value of $\Delta\alpha$ (adopting Level-2 that 0 deg. here), as shown in Table 5.

To verify the convergence of obtained results, the ideal- and worst-case scenarios are also derived with five levels of the manufacturing tolerances in Appendix A, which are the same as the aforementioned results based on three levels of the manufacturing tolerances.

Figure 6 shows the electromagnetic torques in the 6-slot/2-pole modular HSPM motor with the ideal- and worst-case scenarios of manufacturing tolerances. As can be seen, the average

TABLE 5 Ideal and worst-case scenarios of manufacturing tolerances.

	Δg	Δm	$\Delta\alpha$
Ideal	2 (0 mm)	2 (0 mm)	2 (0 deg.)
Worst	3 (0.1 mm)	1 (-0.1 mm)	2 (0 deg.)

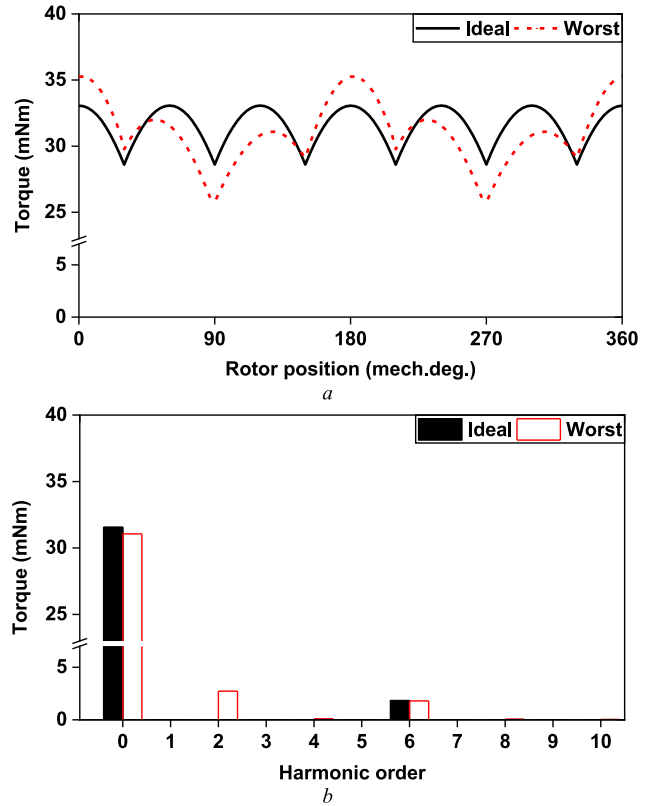


FIGURE 6 Torques of 6-slot/2-pole modular high-speed permanent magnet motor with ideal- and worst-case scenarios of manufacturing tolerances. (a) Waveforms and (b) spectra.

torques are similar, 31.5 and 31 mNm in the machine with the ideal- and worst-case scenarios, respectively. However, the torque ripple has a significant deterioration due to the manufacturing tolerances, from 7.1% to 15.3% in the machine from ideal- to worst-case scenarios of manufacturing tolerances. The main reason is that the second harmonic is almost zero in the machine with the ideal-case scenario, whilst it is increased to 2.7 mNm in the machine with the worst-case scenario.

3.2 | Optimisation of design variables

Since the circumferential positions of the teeth can influence the harmonic components of torque ripple associated with the pole number [23], which is the second harmonic and it is the same order significantly affected by manufacturing tolerances as aforementioned (see Figure 6), they are selected as design variables to suppress the torque ripple due to manufacturing tolerances.

Figure 7 shows the relative tooth circumferential positions (β_1 and β_2) in one segment of the stator in the 6-slot/2-pole modular HSPM motor, while the second segment is rotationally symmetrical to the first one. Without optimisation, the original values of β_1 and β_2 are zero. In optimisation, based on experience, seven levels of β_1 and β_2 , that is, Level-1 (−6 deg.), Level-2 (−4 deg.), Level-3 (−2 deg.), Level-4 (0 deg.), Level-5 (2 deg.), Level-6 (4 deg.), and Level-7 (6 deg.) are adopted to calculate the effectiveness of suppressing torque ripples, as shown in Table 6. Referring to [36], Table 7 shows the L49 orthogonal array for the Taguchi method, which is adopted for evaluating the expected results.

Figure 8 shows the influence of different tooth circumferential positions on the torque ripple. Notably, when the max (T_{ideal} , T_{worst}), that is, the maximum of T_{ideal} and T_{worst} , is the minimum, it means the torque ripples in a machine topology at

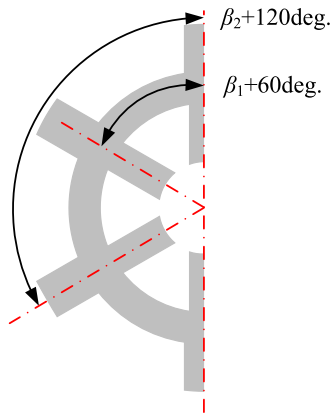


FIGURE 7 Tooth circumferential positions in one stator segment (another stator segment is rotationally symmetrical with this one).

TABLE 6 Seven levels of tooth circumferential positions.

	β_1 (deg.)	β_2 (deg.)
Level-1	−6	−6
Level-2	−4	−4
Level-3	−2	−2
Level-4	0	0
Level-5	2	2
Level-6	4	4
Level-7	6	6

TABLE 7 Layout of the L49 orthogonal array.

	β_1	β_2
1	1	1
2	1	2
...
49	7	7

ideal- and worst-case scenarios of manufacturing tolerances are tradeoffs. To a certain extent, it reflects that the torque ripple will be controlled within a relatively good range across all tolerance ranges. As can be seen, when the combination that (β_1 , β_2) is (0 deg., −4 deg.), it will be the desirable result since max(T_{ideal} , T_{worst}), 10.2%, is the smallest in all potential combinations. Since the original design (see Figure 1) is the symmetrical structure, it is called the original symmetrical machine, whilst the optimised design is called the optimised asymmetric machine due to the asymmetric tooth circumferential positions. Table 8 shows the tooth circumferential positions in the optimised asymmetric machine, with reference to those in the original symmetrical machine.

Since the obtained desirable result is inside the hypothetical ranges of tooth circumferential position, it means the hypothetical ranges are suitable. If one of the obtained desirable results is at the endpoint of the range, the ranges need to be enlarged. Moreover, to verify the convergence of the obtained results, the 13 levels of relative tooth circumferential positions are calculated in Appendix B. The same results are derived from the aforementioned results obtained by seven levels. It is verifying that the obtained result is convergence and is the desirable result.

Figure 9 shows the topology of this optimised asymmetric 6-slot/2-pole HSPM machine. Compared to the original symmetrical topology in Figure 1 ($\beta_1 = \beta_2 = 0$ deg.), only the tooth circumferential positions of this optimised asymmetric topology are different, that is, $\beta_1 = 0$ deg. and $\beta_2 = -4$ deg.

Figure 10 and Table 9 compare the electromagnetic torques in the original symmetrical and optimised asymmetric machines. As can be seen, even though the torque ripple of the machine with the ideal-case scenario is increased from 7.1% to 10.2%, the value (10.2%) is much smaller than the highest

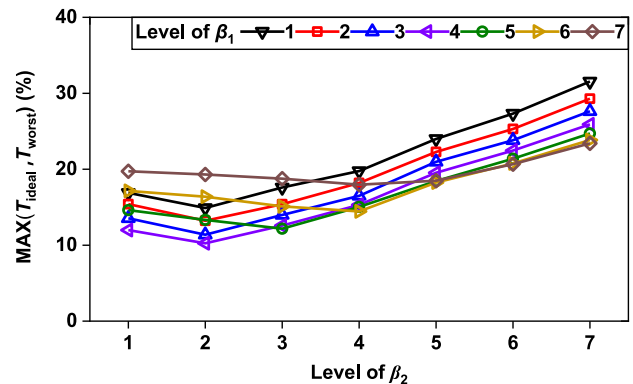


FIGURE 8 Effects and interactions of tooth circumferential positions with seven levels.

TABLE 8 Optimised tooth circumferential positions based on seven levels.

	β_1	β_2
Original	4 (0 deg.)	4 (0 deg.)
Optimised	4 (0 deg.)	2 (−4 deg.)

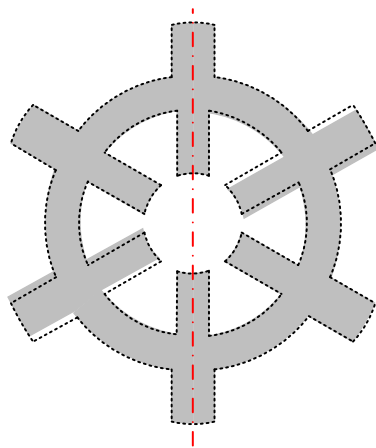


FIGURE 9 Topology of the optimised asymmetric 6-slot/2-pole modular high-speed permanent magnet motor (black dotted line is the original symmetrical topology).

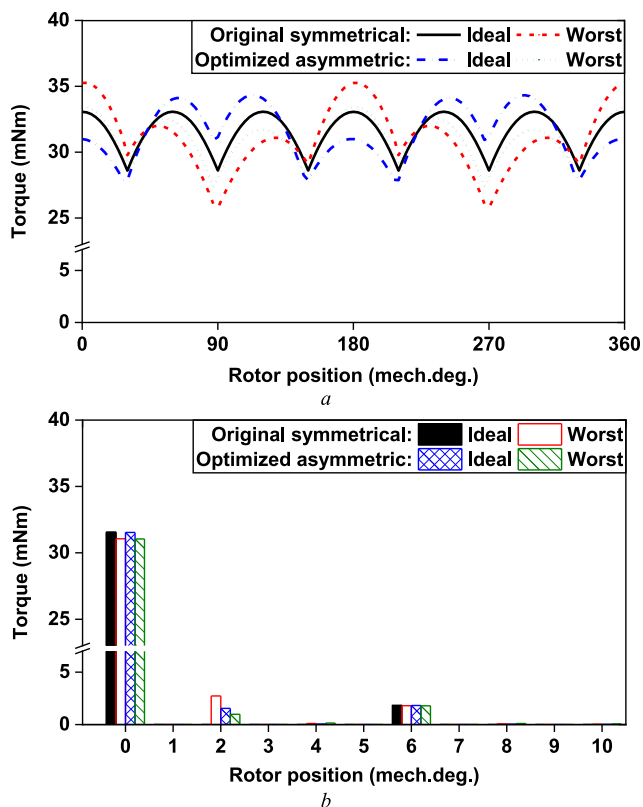


FIGURE 10 Torques in original symmetrical and optimised asymmetric 6-slot/2-pole modular high-speed permanent magnet motors. (a) Waveforms and (b) spectra.

TABLE 9 Average torque and torque ripple in original symmetrical and optimised asymmetric 6-slot/2-pole modular high-speed permanent magnet motors.

	Ideal	Worst
Original	31.6 mNm, 7.1%	31.1 mNm, 15.3%
Optimised	31.5 mNm, 10.2%	31.1 mNm, 9.7%

torque ripple (15.3%) in the original symmetrical machine. Importantly, the torque ripple of the machine with the worst-case scenario is reduced significantly by 40%, from 15.3% to 9.7%. In addition, the average torques are the same in the original symmetrical and optimised asymmetric machines, both of which are 31.5 and 31 mNm in machines with ideal- and worst-case scenarios of manufacturing tolerances, respectively.

Overall, torque ripple is the tradeoff between ideal- and worst-case scenarios without jeopardising average torque. Particularly, torque ripple is significantly reduced by 40% in the machine with the worst-case scenario of manufacturing tolerances.

4 | TORQUE RIPPLE DISTRIBUTIONS OF ORIGINAL SYMMETRICAL AND OPTIMISED ASYMMETRIC MACHINES

Figure 11 shows hypothetical 100 sets Δg , Δm , and $\Delta \alpha$, referring to the distributions of the manufacturing tolerances introduced in Section 2.

As can be seen, blue bars are the distributions of the hypothetical 100 sets of manufacturing tolerances, whilst red lines are the fitted distribution curves. Arbitrarily combining those three manufacturing tolerances, there are 100 groups of the scenarios of the manufacturing tolerances that can be obtained. Notably, the combination of manufacturing tolerances satisfies that $\Delta \alpha$ occurs in the presence of Δg and its maximum range is limited by two stator segments being not contacted.

Figure 12 shows the scatter plots and distribution plots of the average torques of the original symmetrical (see Figure 1) and optimised asymmetric (see Figure 9) 6-slot/2-pole modular HSPM motors with 100 sets of manufacturing tolerances (see Figure 11). The average torques in the optimised asymmetric machine are almost the same to that in the original symmetrical machine.

Figure 13 shows the scatter plots and distribution plots of torque ripples. In Figure 13a, compared to the torque ripple in the original symmetrical machines, torque ripples in the optimised asymmetric machines are lower and closer to the lower limit. Specifically, the maximum of torque ripples is reduced by 33%, from 17.1% to 11.4%, whilst the mean of torque ripples is reduced by 16%, from 11% to 9.3%. Additionally, distribution plots in Figure 13b indicate the lower values, smaller range, and more concentrated distribution of torque ripples in the optimised asymmetric machine.

Overall, the torque ripples are decreased and more concentratedly consistently distributed in the optimised asymmetric 6-slot/2-pole HSPM machines under the hypothetical 100 sets of manufacturing tolerances.

5 | EXPERIMENTAL VALIDATION

To verify the FEA models and the above analyses, two prototypes of the 6-slot/2-pole modular HSPM motor without and with manufacturing tolerances are fabricated. Optimising

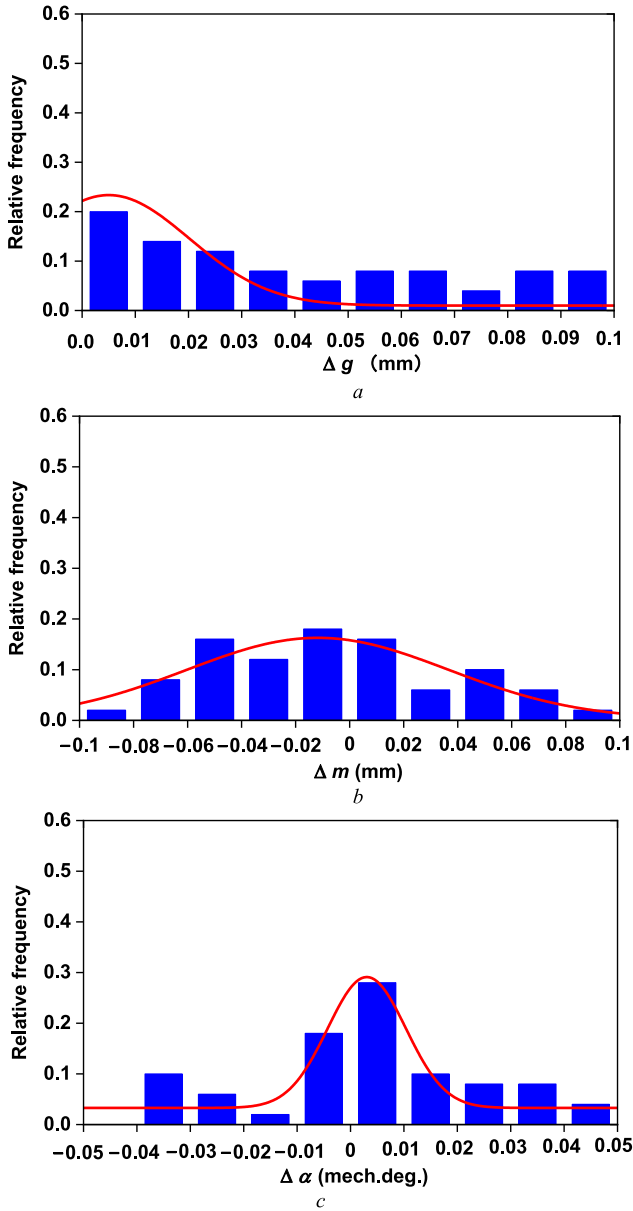


FIGURE 11 Hypothetical 100 set distributions of manufacturing tolerances. (a) Split gap (Δg), (b) misalignment (Δm), and (c) offset angle ($\Delta \alpha$).

tooth circumferential positions to reduce torque ripple depends on the actual ranges of the manufacturing tolerances, necessitating measurements for hundreds of machines in mass production which are not realistic. Thus, these two prototypes are mainly used to verify the FEA models and the effectiveness of the optimisation method.

Figure 14 shows the photos of these two prototypes of the 6-slot/2-pole modular HSPM motor, that is, without manufacturing tolerance and with enlarged manufacturing tolerances ($\Delta g = 1$ mm, $\Delta m = -1$ mm, and $\Delta \alpha = 0$ deg.). Specifically, the phase back-EMFs, cogging torques, and static torques are measured to verify the correctness of the FEA models of the aforementioned analyses. Referring to [40], the measurements are executed.

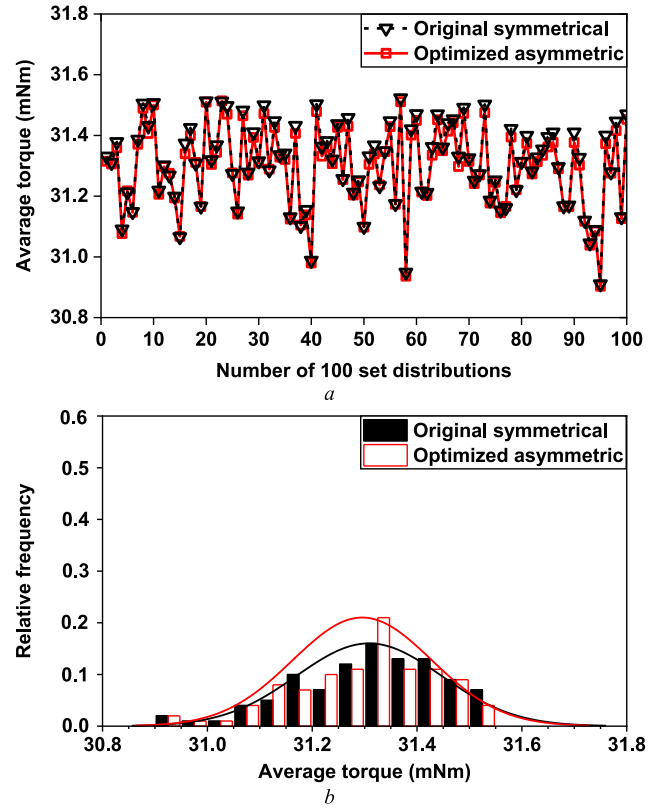


FIGURE 12 Average torques in original symmetrical and optimised asymmetric designs under 100 set distributions of manufacturing tolerances. (a) Scatter plots and (b) distribution plots.

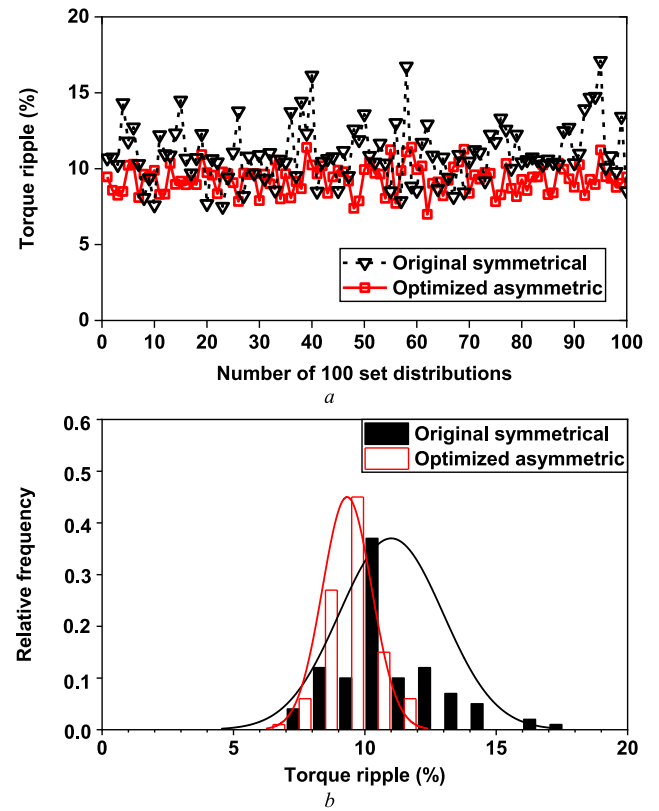


FIGURE 13 Torque ripples in original symmetrical and optimised asymmetric designs under 100 set distributions of manufacturing tolerances. (a) Scatter plots and (b) distribution plots.

5.1 | Back-EMF

Figure 15 shows the phase back-EMFs of the 6-slot/2-pole modular HSPM motors. Firstly, the measured and FEA predicted results are very consistent, verifying the correctness of the FEA models. Secondly, the amplitudes of three phase back-EMFs are almost the same in the machine without manufacturing tolerance. However, they all are reduced and the

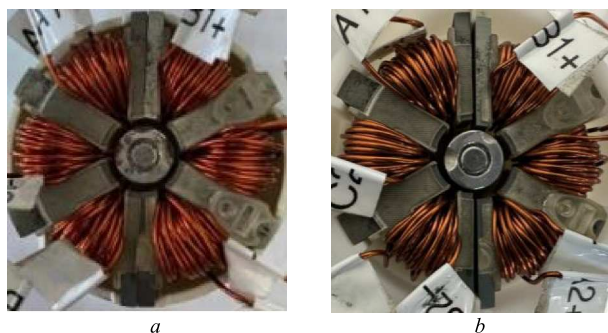
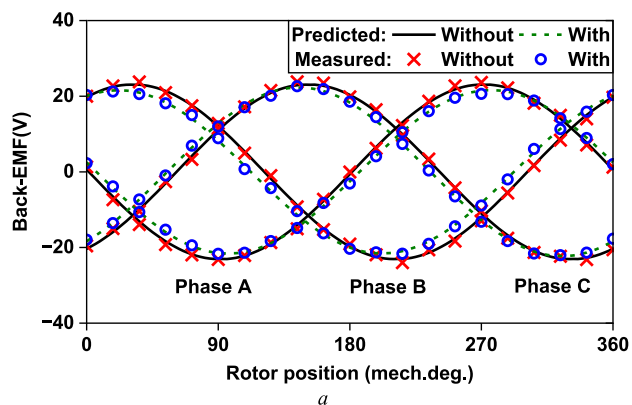


FIGURE 14 Prototypes of 6-slot/2-pole modular high-speed permanent magnet motor. (a) Without manufacturing tolerance and (b) with manufacturing tolerances.



back-EMF of phase B is higher than that of phase A (or C). It indicates manufacturing tolerances result in the lower and unbalanced back-EMFs.

5.2 | Cogging torque

Figure 16 shows the cogging torques of the 6-slot/2-pole modular HSPM motor. The measured and FEA predicted results are very close, the following conclusions can also be achieved.

The cogging torque is almost zero in the machine without manufacturing tolerance, whilst it is 17 mNm of the second harmonic of cogging torque in the machine with manufacturing tolerances. This second harmonic of cogging torque has the main contribution to the torque ripple, as aforementioned analysis in Section 3.

5.3 | Static torque

Figure 17 shows the on-load static torques of the 6-slot/2-pole modular HSPM motor at different rotor positions ($I_A = -I_B = 5A$ and $I_C = 0A$) and different phase currents (rotor

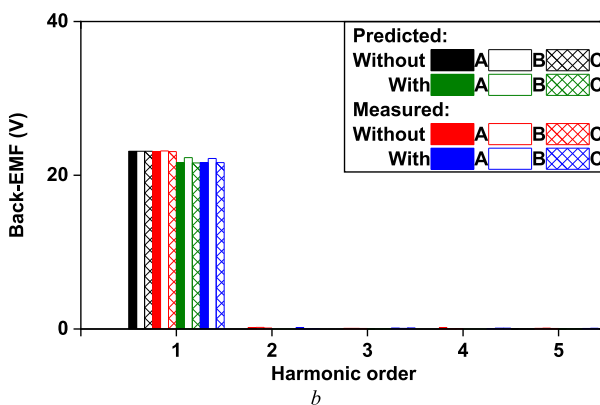


FIGURE 15 Measured and FEA predicted phase back-EMF of 6-slot/2-pole modular HSPM motor without/with manufacturing tolerances ($\Delta g = 1$ mm, $\Delta m = -1$ mm, and $\Delta \alpha = 0$ deg.) at 180k r/min. (a) Waveforms and (b) spectra. EMF, Electromotive Forces; FEA, finite element analysis; HSPM, high-speed permanent magnet.

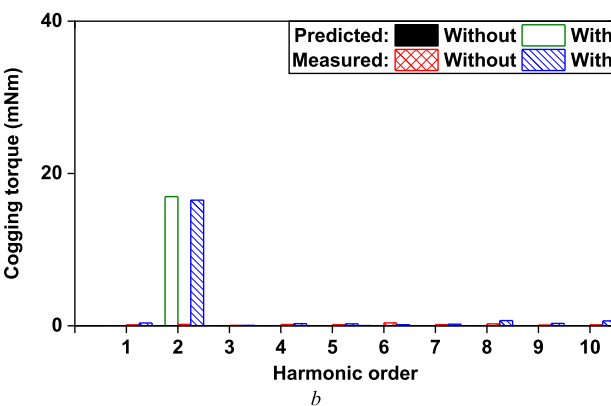
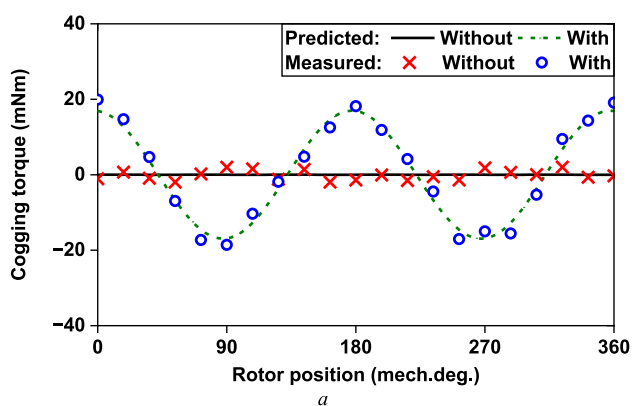


FIGURE 16 Measured and FEA predicted cogging torques of original symmetrical 6-slot/2-pole modular HSPM motor without/with manufacturing tolerances ($\Delta g = 1$ mm, $\Delta m = -1$ mm, and $\Delta \alpha = 0$ deg.). (a) Waveforms and (b) spectra. FEA, finite element analysis; HSPM, high-speed permanent magnet.

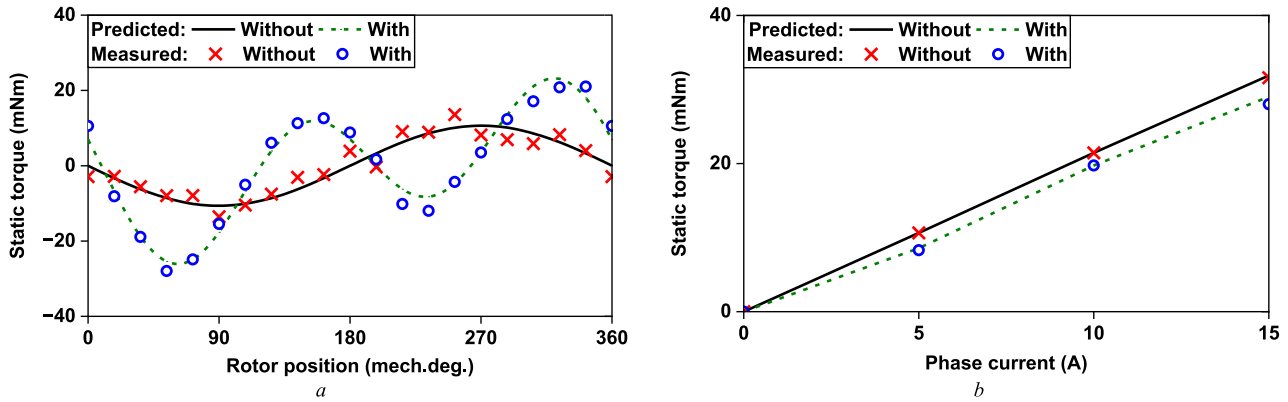


FIGURE 17 Measured and FEA predicted static torque of 6-slot/2-pole modular HSPM motor without/with manufacturing tolerances ($\Delta g = 1$ mm, $\Delta m = -1$ mm, and $\Delta \alpha = 0$ deg.). (a) Different rotor positions ($I_A = -I_B = 5$ A and $I_C = 0$ A) and (b) Different phase currents (rotor position at 270 mech.deg.). FEA, finite element analysis; HSPM, high-speed permanent magnet.

position at 270 mech.deg.), where I_A , I_B , and I_C are armature currents of phases A, B, and C. As can be seen, the measured and FEA predicted results in each case have a good agreement.

Overall, the measured and FEA predicted back-EMFs, cogging torques, and static torques have a good agreement, verifying the correctness of the FEA models in the aforementioned analyses and the effectiveness of the results obtained by the proposed strategy.

6 | CONCLUSION

In this paper, a robust design strategy based on the Taguchi method is proposed, which could significantly reduce the torque ripple of the 6-slot/2-pole modular HSPM motor with manufacturing tolerances in mass production. Based on this strategy, the effects, interactions, and worst-case scenario of manufacturing tolerances (Δg , Δm , and $\Delta \alpha$) on torque ripple can be easily identified, indicating Δg has the highest effect followed by Δm , positive Δg and negative Δm have the strengthening effect and $\Delta \alpha$ does not have effect, and the worst-case scenario is achieved when Δg and Δm are positive and negative maximum values, respectively. Subsequently, the torque ripple is optimised by tooth circumferential positions, considering the tradeoff of torque ripples between ideal- and worst-case scenarios and without jeopardising average torque. Particularly torque ripple is reduced 40% (from 15.3% to 9.7%) in the worst-case scenario.

Moreover, for the hypothetical 100 sets of manufacturing tolerances with Gauss distributions, torque ripples are reduced and their distribution is more concentrated after the optimisation, with 33% and 16% reductions for the maximum and mean values of torque ripples, respectively. Notably, average torques are almost the same.

The FEA models and correctness of this study are verified by the measured phase back-EMFs, cogging torques, and static torques in the prototypes of 6-slot/2-pole modular HSPM motors.

Analyses of other influential variables and rotor eccentricities will be performed in the future.

AUTHOR CONTRIBUTIONS

Dong Xiang: Investigation; methodology; writing—original draft. **Zi Qiang Zhu:** Methodology; project administration; writing—review & editing. **Dawei Liang:** Writing—review & editing. **Fan Xu:** Resources; validation. **Tianran He:** Validation.

CONFLICT OF INTEREST STATEMENT

The authors declare no conflicts of interest.

DATA AVAILABILITY STATEMENT

The data that support the findings of this study are available from the corresponding author upon reasonable request.

ORCID

Dong Xiang <https://orcid.org/0000-0002-0465-3688>
Zi Qiang Zhu <https://orcid.org/0000-0001-7175-3307>
Dawei Liang <https://orcid.org/0000-0002-1574-9810>
Fan Xu <https://orcid.org/0009-0006-7115-5589>
Tianran He <https://orcid.org/0000-0002-4118-0736>

REFERENCES

1. El-Refaié, A.: Fractional-slot concentrated-windings synchronous permanent magnet machines: opportunities and challenges. *IEEE Trans. Ind. Electron.* 57(1), 107–121 (2010). <https://doi.org/10.1109/tie.2009.2030211>
2. Weeber, K., et al.: Advanced permanent magnet machines for a wide range of industrial applications. In: *IEEE PES General Meeting*, pp. 1–6. Minneapolis (2010)
3. Islam, M., Islam, R., Sebastian, T.: Noise and vibration characteristics of permanent magnet synchronous motors using electromagnetic and structural analyses. In: *Proceedings of IEEE Energy Conversion Congress and Exposition (ECCE)*, pp. 3399–3405. Phoenix (2011)
4. Sebastian, T., Slemmon, G., Rahman, M.: Modelling of permanent magnet synchronous motors. *IEEE Trans. Magn.* 22(5), 1069–1071 (1986). <https://doi.org/10.1109/tmag.1986.1064466>

5. Dai, M., Keyhani, A., Sebastian, T.: Torque ripple analysis of a PM brushless DC motor using finite element method. *IEEE Trans. Energy Convers.* 19(1), 40–45 (2004). <https://doi.org/10.1109/tec.2003.819105>
6. Islam, M., et al.: Design considerations of sinusoidally excited permanent-magnet machines for low-torque-ripple applications. *IEEE Trans. Ind. Appl.* 41(4), 955–962 (2005). <https://doi.org/10.1109/tia.2005.851026>
7. Gebregergis, A., et al.: Modeling of permanent-magnet synchronous machine including torque ripple effects. *IEEE Trans. Ind. Appl.* 51(1), 232–239 (2015). <https://doi.org/10.1109/tia.2014.2334733>
8. Singh, A., et al.: A generalized theory to predict the torque harmonics in permanent magnet machines. In: *Proceedings of IEEE Energy Conversion Congress and Exposition (ECCE)*, pp. 3711–3715. Vancouver (2021)
9. Jahns, T., Soong, W.: Pulsating torque minimization techniques for permanent magnet AC motor drives—a review. *IEEE Trans. Ind. Electron.* 43(2), 321–330 (1996). <https://doi.org/10.1109/41.491356>
10. Zhu, Z.Q., Howe, D.: Influence of design parameters on cogging torque in permanent magnet machines. *IEEE Trans. Energy Convers.* 15(4), 407–412 (2000). <https://doi.org/10.1109/60.900501>
11. Bianchi, N., Bolognani, S.: Design techniques for reducing the cogging torque in surface-mounted PM motors. *IEEE Trans. Ind. Appl.* 38(5), 1259–1265 (2002). <https://doi.org/10.1109/tia.2002.802989>
12. Zhu, L., et al.: Analytical methods for minimizing cogging torque in permanent-magnet machines. *IEEE Trans. Magn.* 45(4), 2023–2031 (2009). <https://doi.org/10.1109/tmag.2008.2011363>
13. Islam, M., Islam, R., Sebastian, T.: Experimental verification of design techniques of permanent-magnet synchronous motors for low-torque-ripple applications. *IEEE Trans. Ind. Appl.* 47(1), 88–95 (2011). <https://doi.org/10.1109/tia.2010.2091612>
14. Chu, W., Zhu, Z.Q.: Reduction of on-load torque ripples in permanent magnet synchronous machines by improved skewing. *IEEE Trans. Magn.* 49(7), 3822–3825 (2013). <https://doi.org/10.1109/tmag.2013.2247381>
15. Wang, K., Zhu, Z.Q., Ombach, G.: Torque enhancement of surface-mounted permanent magnet machine using third-order harmonic. *IEEE Trans. Magn.* 50(3), 104–113 (2014). <https://doi.org/10.1109/tmag.2013.2286780>
16. Wang, K., et al.: Average torque improvement of interior permanent-magnet machine using third harmonic in rotor shape. *IEEE Trans. Ind. Electron.* 61(9), 5047–5057 (2014). <https://doi.org/10.1109/tie.2013.2286085>
17. Qi, J., et al.: Suppression of torque ripple for consequent pole PM machine by asymmetric pole shaping method. *IEEE Trans. Ind. Appl.* 58(3), 3545–3557 (2022). <https://doi.org/10.1109/tia.2022.3159629>
18. Zhou, T., Shen, J.: Cogging torque and operation torque ripple reduction of interior permanent magnet synchronous machines by using asymmetric flux-barriers. In: *20th International Conference on Electrical Machines and Systems (ICEMS)*, pp. 1–6. Sydney (2017)
19. Xiao, Y., et al.: A novel spoke-type asymmetric rotor interior permanent magnet machine. *IEEE Trans. Ind. Appl.* 57(5), 4840–4851 (2021). <https://doi.org/10.1109/tia.2021.3099452>
20. Peng, G., et al.: Improved V-shaped interior permanent magnet rotor topology with inward-extended bridges for reduced torque ripple. *IET Electr. Power Appl.* 14(12), 2404–2411 (2020). <https://doi.org/10.1049/iet-epa.2019.0850>
21. Islam, M., Mir, S., Sebastian, T.: Issues in reducing the cogging torque of mass-produced permanent-magnet brushless DC motor. *IEEE Trans. Ind. Appl.* 40(3), 813–820 (2004). <https://doi.org/10.1109/tia.2004.827469>
22. Zhu, Z.Q., Azar, Z., Ombach, G.: Influence of additional air gaps between stator segments on cogging torque of permanent-magnet machines having modular stators. *IEEE Trans. Magn.* 48(6), 2049–2055 (2012). <https://doi.org/10.1109/tmag.2011.2179667>
23. Yang, Y., et al.: A method to estimate the worst-case torque ripple under manufacturing uncertainties for permanent magnet synchronous machines. In: *Proceedings of IEEE Energy Conversion Congress and Exposition (ECCE)*, pp. 4075–4082 (2020)
24. Li, G., Ren, B., Zhu, Z.Q.: Cogging torque and torque ripple reduction of modular permanent magnet machines. In: *Proceedings of 22nd International Conference on Electrical Machines (ICEM)*, pp. 193–199. Lausanne (2016)
25. Shi, Z., et al.: Robust design optimization of a five-phase PM hub motor for fault-tolerant operation based on Taguchi method. *IEEE Trans. Energy Convers.* 35(4), 2036–2044 (2020). <https://doi.org/10.1109/tec.2020.2989438>
26. Paul, S., et al.: Robust design approach of permanent magnet synchronous motors for torque ripple minimization. In: *Proceedings of 11th IEEE International Electric Machines & Drives Conference (IEMDC)*, pp. 1280–1287 (2019)
27. Islam, M., et al.: Cogging torque minimization in pm motors using robust design approach. *IEEE Trans. Ind. Appl.* 47(4), 1661–1669 (2011). <https://doi.org/10.1109/tia.2011.2154350>
28. Lee, S., et al.: Optimal design of interior permanent magnet synchronous motor considering the manufacturing tolerances using Taguchi robust design. *IET Electr. Power Appl.* 8(1), 23–28 (2014). <https://doi.org/10.1049/iet-epa.2013.0109>
29. Kim, K., et al.: Taguchi robust optimum design for reducing the cogging torque of EPS motors considering magnetic unbalance caused by manufacturing tolerances of PM. *IET Electr. Power Appl.* 10(9), 909–915 (2016). <https://doi.org/10.1049/iet-epa.2015.0638>
30. Kim, K., Lee, B.: Taguchi robust design for the multi-response considering the manufacturing tolerance used in high-speed air blower motor. *IET Electr. Power Appl.* 14(7), 1141–1147 (2020). <https://doi.org/10.1049/iet-epa.2019.0600>
31. Kim, K., Lee, B.: Taguchi's robust design optimization of water-cooled ISG motors considering manufacturing tolerances. *IET Electr. Power Appl.* 14(5), 865–871 (2020). <https://doi.org/10.1049/iet-epa.2019.0574>
32. Chowdhury, M., et al.: Robust design optimization of permanent magnet synchronous machine utilizing genetic and Taguchi's algorithm. In: *Proceedings of IEEE Energy Conversion Congress and Exposition (ECCE)*, pp. 5006–5012. Denver (2013)
33. Islam, M., Pramanik, A.: Comparison of design of experiments via traditional and Taguchi method. *J. Adv. Manuf. Syst.* 15(3), 151–160 (2013). <https://doi.org/10.1142/s0219686716500116>
34. Feng, H., et al.: Torque ripple reduction of brushless DC motor with convex arc-type permanent magnets based on robust optimization design. *IET Electr. Power Appl.* 16(5), 565–574 (2022). <https://doi.org/10.1049/elp2.12176>
35. Mathews, P.: *Design of Experiments with MINITAB*. ASQ Quality Press, Milwaukee (2005)
36. Mori, T.: *Taguchi Methods: Benefits, Impacts, Mathematics, Statistics, and Applications*. American Society of Mechanical Engineers, New York (2011)
37. Shigematsu, K., et al.: The study of eddy current in rotor and circuit coupling analysis for small size and ultra-high speed motor. In: *Proceedings of International Power Electronics and Motion Control Conference (IPEMC)*, pp. 275–279. Xi'an (2004)
38. Noguchi, T., et al.: 220,000-r/min, 2-kw PM motor drive for turbo-charger. *Electr. Eng. Jpn.* 161(3), 31–40 (2007)
39. Lim, M., et al.: Design of an ultra-high-speed permanent-magnet motor for an electric turbocharger considering speed response characteristics. *IEEE ASME Trans. Mechatron.* 22(2), 774–784 (2017). <https://doi.org/10.1109/tmech.2016.2634160>
40. Xu, F., et al.: Influence of stator gap on electromagnetic performance of 6-slot/2-pole modular high-speed permanent magnet motor with toroidal windings. *IEEE Access* 9, 94470–94494 (2021). <https://doi.org/10.1109/access.2021.3092053>
41. He, T., et al.: 6-slot/2-pole permanent magnet motors with non-overlapping two coil-pitch windings for ultra-high-speed applications. In: *2023 IEEE Transportation Electrification Conference and Expo, Asia-Pacific (ITEC Asia-Pacific)*, pp. 1–7. Chiang Mai (2023)

42. Xu, F., et al.: Investigation of optimal split ratio of 6-slot/2-pole high speed permanent magnet motor with toroidal winding. *CES Trans. Electr. Mach. Sys.* 6(4), 343–351 (2022). <https://doi.org/10.30941/cestems.2022.00045>
43. He, T., et al.: Comparison of toroidal and tooth-coil winding 2-pole slotted high-speed permanent magnet motors. *IEEE Trans. Ind. Appl.* 60(3), 3870–3882 (2024). <https://doi.org/10.1109/tia.2024.3366500>
44. Kim, T., et al.: Tolerance study to forecast performances of permanent magnet synchronous machines using segmented stator for mass production. *IEEE Trans. Ind. Appl.* 54(5), 4333–4342 (2018). <https://doi.org/10.1109/tia.2018.2844200>

How to cite this article: Xiang, D., et al.: Taguchi-based robust design for minimising torque ripple in 6-slot/2-pole modular high-speed permanent magnet motor with manufacturing tolerances. *IET Electr. Power Appl.* 1–13 (2024). <https://doi.org/10.1049/elp2.12490>

APPENDIX A: FIVE LEVELS OF MANUFACTURING TOLERANCES

To demonstrate that the three-level manufacturing tolerances are adequate in predicting the highest torque ripple, the five-level manufacturing tolerances in the 6-slot/2-pole modular HSPM motor are evaluated, with the same process shown in Part A of Section 3.

Tables A1 and A2 show the five levels of the manufacturing tolerances and the L125 orthogonal array in the Taguchi method [23]. After calculating, Figure A1 shows the effects and the interactions under five levels of each manufacturing tolerance, and subsequently, the worst-case scenario is obtained as shown in Table A3. As can be seen, the same results of Table A3 can be obtained with that in Table 5 (see Part A of Section 3), verifying the convergent results for the worst-case scenario of manufacturing tolerances when three levels are used for these manufacturing tolerances.

TABLE A1 Five levels of manufacturing tolerances.

	Level-1	Level-2	Level-3	Level-4	Level-5
Δg , mm	0	0.025	0.05	0.075	0.1
Δm , mm	-0.1	-0.05	0	0.05	0.1
$\Delta \alpha$, mech.deg.	-0.05	-0.025	0	0.025	0.05

TABLE A2 Layout of the L125 orthogonal array.

	Δg , mm	Δm , mm	$\Delta \alpha$, deg.
1	1	1	1
2	1	1	2
...
125	5	5	5

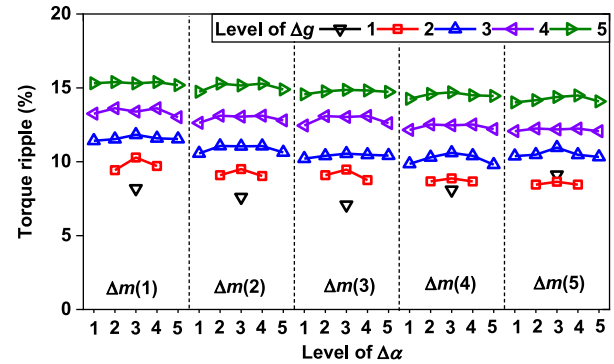


FIGURE A1 Effects and interactions of manufacturing tolerances with five levels.

TABLE A3 Ideal and worst-case scenarios of manufacturing tolerances based on five levels.

	Δg	Δm	$\Delta \alpha$
Ideal	5 (0 mm)	3 (0 mm)	3 (0 deg.)
Worst	5 (0.1 mm)	1 (-0.1 mm)	3 (0 deg.)

APPENDIX B: THIRTEEN LEVELS OF TOOTH CIRCUMFERENTIAL POSITIONS

To verify the convergence results obtained from the seven levels of tooth circumferential positions, the 13 levels of tooth circumferential positions are evaluated in the 6-slot/2-pole modular HSPM motor.

Tables B1 and B2 show the 13 levels and L169 orthogonal array [23]. Figure B1 shows the effects and interactions, and subsequently, the optimised tooth circumferential positions are obtained as shown in Table B3, which is the same as Table 8 (see Part B of Section 3), verifying the convergent results and correctness in Part B of Section 3.

TABLE B1 Thirteen levels of tooth circumferential positions.

	β_1 (deg.)	β_2 (deg.)
Level-1	-6	-6
Level-2	-5	-5
Level-3	-4	-4
Level-4	-3	-3
Level-5	-2	-2
Level-6	-1	-1
Level-7	0	0
Level-8	1	1
Level-9	2	2
Level-10	3	3
Level-11	4	4
Level-12	5	5
Level-13	6	6

TABLE B2 Layout of the L169 orthogonal array.

	β_1	β_2
1	1	1
2	1	2
...
169	13	13

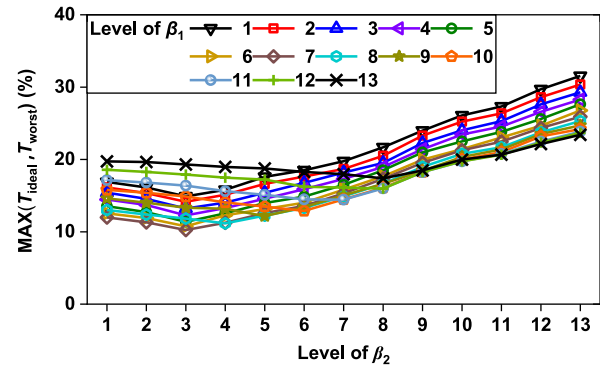


FIGURE B1 Effects and interactions of tooth circumferential positions with 13 levels.

TABLE B3 Optimised tooth circumferential positions based on 13 levels.

	β_1	β_2
Original	7 (0 deg.)	7 (0 deg.)
Optimised	7 (0 deg.)	3 (-4 deg.)